RESEARCH

Tumor-associated macrophage-derived itaconic acid contributes to nasopharyngeal carcinoma progression by promoting immune escape via TET2

Xiaowei Zhang[1], Shen'er Qian[1], Ping'an Wu[2], Benquan Yu[3], Danhui Yin[3], Xia Peng[3], Shisheng Li[3,4,5], Zian Xiao[3,4,5] and Zuozhong Xie[3,4,5*]

Abstract

Nasopharyngeal carcinoma (NPC) is a malignant tumor of epithelial origin in head and neck with high incidence rate in South China, Southeast Asia and North Africa. The intervention of tumor-associated macrophages (Mφs) (TAMs)-mediated immunosuppression is a potential therapeutic strategy against tumor metastasis, but the exact mechanisms of TAM-mediated immunosuppression in nasopharyngeal carcinoma are unclear. Furthermore, how TAM affects the occurrence and development of nasopharyngeal carcinoma through metabolism is rarely involved. In this work, we revealed that NPC cells promoted M2-type Mφ polarization and elevated itaconic acid (ITA) release. Also, TAMs facilitated NPC cell proliferation, migration, and invasion through immune response gene 1 (IRG1)-catalyzed ITA production. Then, IRG1-mediated ITA production in TAMs repressed the killing of CD8$^+$ T cells, induced M2-type polarization of TAMs, and reduced the phagocytosis of TAMs. Moreover, we demonstrated ITA played a tumor immunosuppressive role by binding and dampening ten-eleven translocation-2 (TET2) expression. Finally, we proved that ITA promotes NPC growth by facilitating immune escape in CD34$^+$ hematopoietic stem cell humanized mice. In Conclusion, TAM-derived ITA facilitated NPC progression by enhancing immune escape through targeting TET2, highlighting that interfering with the metabolic pathway of ITA may be a potential strategy for NPC treatment.

Keywords Tumor-associated macrophages, Itaconic acid, Nasopharyngeal carcinoma, Immune escape, TET2

*Correspondence:
Zuozhong Xie
zuozhongxie@csu.edu.cn
[1] Department of Otorhinolaryngology Head and Neck Surgery, The Third Xiangya Hospital, Central South University, Changsha, Hunan, China
[2] Department of Otorhinolaryngology Head and Neck Surgery, The University of Hongkong- Shenzhen Hospital, Shenzhen, Guangzhou, China
[3] Department of Otorhinolaryngology Head and Neck Surgery, The Second Xiangya Hospital, Central South University, Changsha 410011, Hunan, China
[4] Laboratory of Otorhinolaryngology Head and Neck Cancer, The Second Xiangya Hospital, Central South University, Changsha, Hunan Province, China
[5] Institute of Otology, Central South University, Changsha, Hunan Province, China

Introduction

Nasopharyngeal carcinoma (NPC) is a group of malignant tumors originating from the epithelial cells of the nasopharyngeal mucosa, with highly invasive and metastatic properties [1]. Statistically, over 130,000 new cases of NPC are diagnosed worldwide each year, and approximately 70% of the patients are in advanced stages with distant metastasis at the time of initial diagnosis, posing a great threat to human health [2]. Tumor microenvironment (TME) provides the conditions for the process of tumor genesis and growth, and it is also the venue in which the body's immune system plays a battle with the tumor [3]. TME can induce an immunosuppressive effect

Zhang *et al. Cell Communication and Signaling*   (2024) 22:413

Page 2 of 18

by suppressing T-cell anti-tumor immunity, prompting tumor cell immune escape, thus leading to tumor metastasis [4].

Tumor-associated macrophages (Mφs) (TAMs), the most numerous immune cells in the TME, play a critical regulatory function in tumor malignant progression [5]. Tumor-regulating effects of TAMs rely on their heterogeneity. One of them, M1-type TAMs amplify the immune response by secreting pro-inflammatory factors, thereby exerting a tumor-suppressive effect [6]. While M2-type TAMs mainly mediate the immunosuppressive effect through the secretion of anti-inflammatory factors, thereby playing a pro-tumorigenic effect [7]. Moreover, TAM can secrete various types of immunosuppressive enzymes to restrain the immune response of cytotoxic T lymphocytes (CTLs) [8]. Therefore, the intervention of TAM-mediated immunosuppression is a potential therapeutic strategy against tumor metastasis, but the exact mechanisms of TAM-mediated immunosuppression are unclear [9].

Itaconic acid (ITA) is a vital effector molecule within the endogenous immune system, and the immune response gene 1 (IRG1) protein links metabolism to immunity by catalyzing ITA production [10]. Mφs synthesize and secrete ITA in response to stress, and the synthesized ITA exerts an anti-inflammatory effect by inhibiting the production of pro-inflammatory cytokines, so it may exert an immunosuppressive effect. Zhao et al. uncovered that IRG1-mediated ITA production in Mφs possesses a tumor-promoting effect [11]. Moreover, IRG1-induced ITA promotes tumorigenesis by the exhaustion of CD8$^+$ T cells [12, 13]. Currently, there are few studies investigating the effect of ITA in NPC and the mechanisms associated with it.

Therefore, we demonstrated that NPC cells promote M2-type Mφ polarization and ITA production. Also, TAMs facilitated NPC cell proliferation, migration, and invasion through IRG1-catalyzed ITA production. Moreover, IRG1-catalyzed ITA production promoted M2-type polarization of TAMs as well as reduced CD8$^+$ T cell killing by interacting and repressing ten-eleven translocation-2 (TET2). Importantly, the promoting effect of ITA on NPC was dependent on immunosuppression. Therefore, this study supports that targeting the metabolic pathways that produce ITA may be a potential strategy for the treatment of NPC.

Methods and materials
Cell culture
Human nasopharyngeal epithelial cells NP69SV40T (NECs) (Catalog No. CL-0804; Pricella, Wuhan, China) were cultured in a cell-specific medium (Catalog No. CM-0804; Pricella). Human NPC cell lines HNE2

(Catalog No. IM-H434; Immocell, Xiamen, China) and HK-1 (Catalog No. CC0708; Cellcook, Guangzhou, China) were cultured in Dulbecco's modified eagle medium (Thermo, Waltham, MA, USA) or Roswell Park Memorial Institute (RPMI)-1640 medium (Sigma, St. Louis, MO, USA) supplemented with 10% fetal bovine serum (FBS, Thermo) and 1% penicillin-streptomycin (P/S, Pricella), respectively. Human THP-1 monocytes (Catalog No. CL-0233; Pricella) were cultured in RPMI-1640 supplemented with 10% FBS, 0.05mM β-mercaptoethanol (Sigma), and 1% P/S. All cells were incubated in a 37 °C incubator (Thermo) with 5% CO_2 environment.

Mφ polarization
To induce M0-type Mφs, about 1×10^6 THP-1 monocytes were stimulated with phorbol 12-myristate 13-acetate (PMA, 185 ng/mL, Sigma) for 6 hours. To induce M2-type polarization, THP-1 monocyte-derived M0-type Mφs were subjected to interleukin (IL)-4 (20 ng/mL, Sigma) and IL-13 (20 ng/mL, Sigma) stimulation for 48 h.

Cell transfection
THP-1 monocytes were transfected with different small interfering RNAs (siRNAs) (si-NC, si-IRG1#1, si-IRG1#2, si-IRG1#3, si-TET2#1, si-TET2#2, or si-TET2#3) (GenePharma, Shanghai, China) using the HiPerFect Transfection Reagent (Qiagen, Hilden, Germany) in an Opti-MEM serum-free medium. Transfected cells were cultured in the appropriate medium for 24 h.

Cell co-culture
To analyze the influence of HK-1 cells on the polarization of Mφs, M0 type Mφs obtained by stimulating THP1 cells with PMA were used for co-culture. The experiment was divided into the following 4 groups: control (mono-cultured M0-type Mφs), M2 stimulation (mono-cultured M0-type Mφs stimulated with IL-4 and IL-13), NEC co-culture (M0-type Mφs co-cultured with NECs), and NPC co-culture (M0-type Mφs co-cultured with HK-1 cells). A non-contact co-culture transwell® system (Catalog No. 3450, Corning, USA) was employed to construct a co-culture system of NPC cells or NECs and Mφ.

To investigate whether IRG1-induced ITA production in TAMs mediates NPC cell malignant behaviors, the experiment was divided into the following 5 groups: control, ITA, TAM-si-NC, TAM-si-IRG1, and TAM-si-IRG1+ITA groups. The ITA solution (5 mM) (Abmole, Shanghai, China) was prepared by dissolving 5 mg of ITA in 7.6864 mL of double-distilled water. For the control group, NPC cells (about 1×10^4/compartment) were seeded into the upper compartments and cultured with

Zhang *et al. Cell Communication and Signaling*   (2024) 22:413

Page 3 of 18

a normal medium added with phosphate-buffered saline (PBS). For the ITA group, NPC cells (about 1×10^4/compartment) were seeded into the upper compartments and stimulated with ITA (125 μM). For the TAM-si-NC and TAM-si-IRG1 groups, the upper compartments were cultured the same as the control group, but the lower compartments were cultured with TAMs transfected with si-NC or si-IRG1. For the TAM-si-IRG1+ITA group, the upper compartments were cultured as in the ITA group, but the lower compartments were cultured as in the TAM-si-IRG1 group. The amount of PBS was the same as ITA.

For analysis of the function of TET2, M0-type Mφs were divided into the following groups: control, ITA, si-TET2, and si-TET2+ITA groups. For the control group, PBS-treated NPC cells were co-cultured with M0-type Mφs. For the ITA group, ITA-stimulated NPC cells were co-cultured with M0-type Mφs. For the si-TET2 group, PBS-treated NPC cells were co-cultured with si-TET2-transfected M0-type Mφs. For the si-TET2+ITA group, ITA-stimulated NPC cells were co-cultured with si-TET2-transfected M0-type Mφs. **Flow cytometry assay**.

Harvested Mφs were made into single-cell suspensions by trypsin digestion. After washing, Mφs were stained with CD206 APC (Catalog No. 141714, Biolegend, San Diego, California, USA) on ice away from light according to the manufacturer's instructions. Flow cytometry analysis was performed on a BD FACSCanto II system (BD Biosciences, Frank, New Jersey, USA) and data were analyzed with FlowJo v10 software (FlowJo, Ashland, OR, USA).

Western blot

Proteins were isolated using RIPA buffer (Catalog No. P0013C, Beyotime, Shanghai, China), and the samples were quantified using the BCA kit (Catalog No. 23227). Equal amounts of total protein were separated and transferred to PVDF membranes. The membrane was blocked with 5% nonfat milk, followed by incubation overnight at 4 °C with antibodies against CD206 (Catalog No. FNab09812, Fine Biotech Co., Ltd, Wuhan, China), arginase-1 (Arg-1) (Catalog No. PA1783, Boster, Wuhan, China), IRG1 (Catalog No. 17805 S, Cell Signaling Technology, USA), β-actin (Catalog No. FNab00869, Fine Biotech Co., Ltd), and TET2 (Catalog No. orb537560, Biorbyt, Wuhan, China). After incubation with secondary antibodies, an ECL kit (Tanon, Shanghai, China) was utilized for the detection of protein bands.

Enzyme-linked immunosorbent assay (ELISA)

The levels of IL-6, IL-10, and vascular endothelial growth factor (VEGF) in different culture media were estimated by the corresponding reagent kit as described by the manufacturer. Information on the kits used for this experiment is shown in Table 1.

Gas chromatography-mass spectrometry (GC-MS)

The levels of ITA in cell culture supernatant samples were measured according to a previous report [14]. Extracellular metabolites were extracted using the ice-cold methanol/water plus internal standard mixture (5:1, v/v). For quantification, GC-MS measurements were performed in selected ion monitoring mode on an Agilent 7890 A GC coupled to an Agilent 5975 C inert XL Mass Selective Detector (Agilent Technologies, Santa Clara, California, USA) using the following masses: m/z 301.2; 343.2; 358.2 (dwell times: 60 ms).

Reverse transcription-quantitative PCR (RT-qPCR)

Total RNA was extracted using Trizol (Catalog No. 15596-026, Ambion, Austin, Texas, USA). Total RNA (2 μg) was reverse transcribed using the Primescript™ RT reagent kit (Catalog No. RR047A, Takala, Dalian, China). The reaction of qPCR was executed with the TB Green® Premix Ex Taq™ II (Catalog No. RR820A, Takara). Relative mRNA levels were computed by the $2^{-\Delta\Delta Ct}$ method [15]. Sequences for all primers are provided in Table 2.

Colony formation assay

NPC cells were co-cultured with TAMs for 14 days. Fixation in 4% paraformaldehyde (Solarbio, Beijing, China) and then staining with 0.1% crystal violet (Solarbio) was performed on colonies. Images were photographed and

Table 1 Information on the kits used for ELISA

Items	Manufacturer	Catalog No.
IL-6	Thermo Fisher Scientific	EH2IL6
IL-10	Sino Biological, Inc.	KIT10947A
VEGF	Sino Biological, Inc.	SEK10008
IFN-γ	MyBioSource.com	MBS262163

Table 2 The sequences of all primers utilized for RT-qPCR

Genes	Sequences	
IRG1	Forward	CCACAGCCAGCAGGTCAATA
	Reverse	TAAGGCTTTCCACCGTGTCC
TET2	Forward	ACAAATGACAGCACAACCGC
	Reverse	GGGTGTGGATGGGTGGTAAG
GAPDH	Forward	GAGAGTGTTTCCTCGTCCCG
	Reverse	ACTGTGCCGTTGAATTTGCC

counted per four fields under an Olympus BX51 microscope (Olympus, Tokyo, Japan).

Wound healing assay

NPC cells were plated in the upper compartments. After 24 h, a scraped cell-free area was made using a micropipette tip (200 μL) and serum-free medium was added, and the lower compartments were seeded with TAMs. Wound closure was observed and photographed at 0 and 24 h, followed by analyzing using the ImageJ software.

Transwell invasion assay

The upper compartment was added with 100 μL of Matrigel (BD Biosciences) and incubated for 4 hours at 37 °C. NPC cells (1×10^4 cells) resuspended in 200 μL of serum-free medium were seeded in the upper compartments, and the upper compartments were seeded with TAMs. After 24 h, the migrated cells were fixed with 4% paraformaldehyde and stained with 0.5% crystal violet. The cells were pictured by a microscope and counted using ImageJ.

T-cell functional assay

$CD8^+$ T cells were generated from the spleen of OT-I mice using the EasySep™ mouse $CD8^+$ T-cell isolation kit (Catalog No. 19853, STEMCELL, USA), followed by stimulating with anti-CD28 (5 mg/mL, Catalog No. BE0015-1, Bioxcell, Beijing, China) and anti-CD3 (0.5 mg/mL, Catalog No. BE0001-1, Bioxcell) pre-coated plates for 2 days and maintained in RPMI-1640 medium with 2-mercaptoethanol (50 mM, Catalog No. M6250, Sigma) and 1% ITS (50 mM, Catalog No. I3146, Sigma). T cells were expanded with IL-2 (0.4 ng/mL, Catalog No. 402-ML-020, R&D Syetems, Minnesota, USA). SIINFEKL peptide (Catalog No. HY-P1489, MCE, USA) was overexpressed in NPC cells in order to work as target cells.

For the T cell killing assay, NPC cells expressing SIINFEKL were co-cultured with $CD8^+$ T treated with different conditioned medium (CM) from control, ITA, TAM-si-NC, TAM-si-IRG1, and TAM-si-IRG1 + ITA groups and allowed to growth for 2 days. For apoptosis analysis, NPC cells were double-stained with annexin V-FITC and propidium iodide (Catalog No. C1062L, Beyotime) according to the manufacturer's instructions, and staining was detected using a BD FACSCanto II system flow cytometer (BD Biosciences).

For the production of luciferase reporter cells, 293T cells were co-transfected with pHIV-luc-zsgreen (Catalog No. 39196, Addgene, Massachusetts, USA), psPAX2 (Catalog No. 12260, Addgene), and pMD2.G (Catalog No. 12259, Addgene) plasmids. Seventy-two hours later, lentivirus was collected and filtered (0.45 mM filter). Lentivirus with pHIV-luc-zsgreen was utilized for the infection of SIINFEKL-expressing NPC cells. For analyzing the killing of T cells, the medium was removed after co-culturing target cells with T cells. Target cells were incubated individually in the blank group. D-luciferin (150 mg/mL, Sigma) was then added and incubated for 10 min. Measurement of luciferase activity was performed by a FLUOstar OPTIMA microplate reader (BMG LABTECH, Germany). Calculation of T cell killing capacity was as follows: cell lysis (%) = (value $_{blank}$-value $_{detection}$)/value $_{blank}$.

For the detection of interferon-gamma (IFN-γ) levels in supernatants, the ELISA MAX standard set mouse IFN-γ kit (Catalog No. MBS262163, MyBiosource Inc., California, USA) was used in accordance with the operating procedures.

Mφ phagocytosis

For the phagocytosis analysis, Mφs in control, TAM-si-NC, TAM-si-IRG1, and TAM-si-IRG1 + ITA groups were cultured for 24 h, followed by incubation with NPC cells labeled with MitoTracker Deep Red for 10 min. The control group was set up with the mono-culture of M0-type Mφs, and the other groups were consistent with the co-cultures described above. After washing, the fluorescent fractions within the Mφs were quantified by flow cytometry.

Animal experiments

All animal experiments were performed on 4-6-week-old mice (Gem Pharmatech (Nanjing, China), including huHSC-NCG ($n=24$) and BALB/c ($n=12$) mice. Mice were maintained under specific pathogen-free conditions

(See figure on next page.)

Fig. 1 NPC cells evoked M2-type polarization of Mφs and facilitated ITA release from Mφs. **A** Schematic diagram illustrating cell mono- and co-culture systems. **B** The proportion of M2-polarized cells in control (mono-culture of THP-1 monocytes), M2 stimulation (THP-1 monocytes stimulated with IL-4 plus IL-13), NEC co-culture (THP-1 monocytes co-cultured with NECs), and NPC co-culture (THP-1 monocytes co-cultured with HK-1 cells) groups was detected by flow cytometry analysis. **C** Protein levels of Arg-1 and CD206 in THP-1 monocytes with different culture systems as described above. **D-F** ELISA detection of TAMs-associated cytokines (IL-6, IL-10, and VEGF) in cell supernatants derived from different THP-1 monocyte culture systems. **G** Concentration of ITA in cell supernatants derived from different THP-1 monocyte culture systems was detected by GC-MS. Data are expressed as means ± SEM and analyzed by one-way ANOVA (***$P < 0.001$, **$P < 0.01$, and *$P < 0.05$ vs. control; ns, no significance; ###$P < 0.001$, ##$P < 0.01$, and #$P < 0.05$ vs. M2 stimulation)
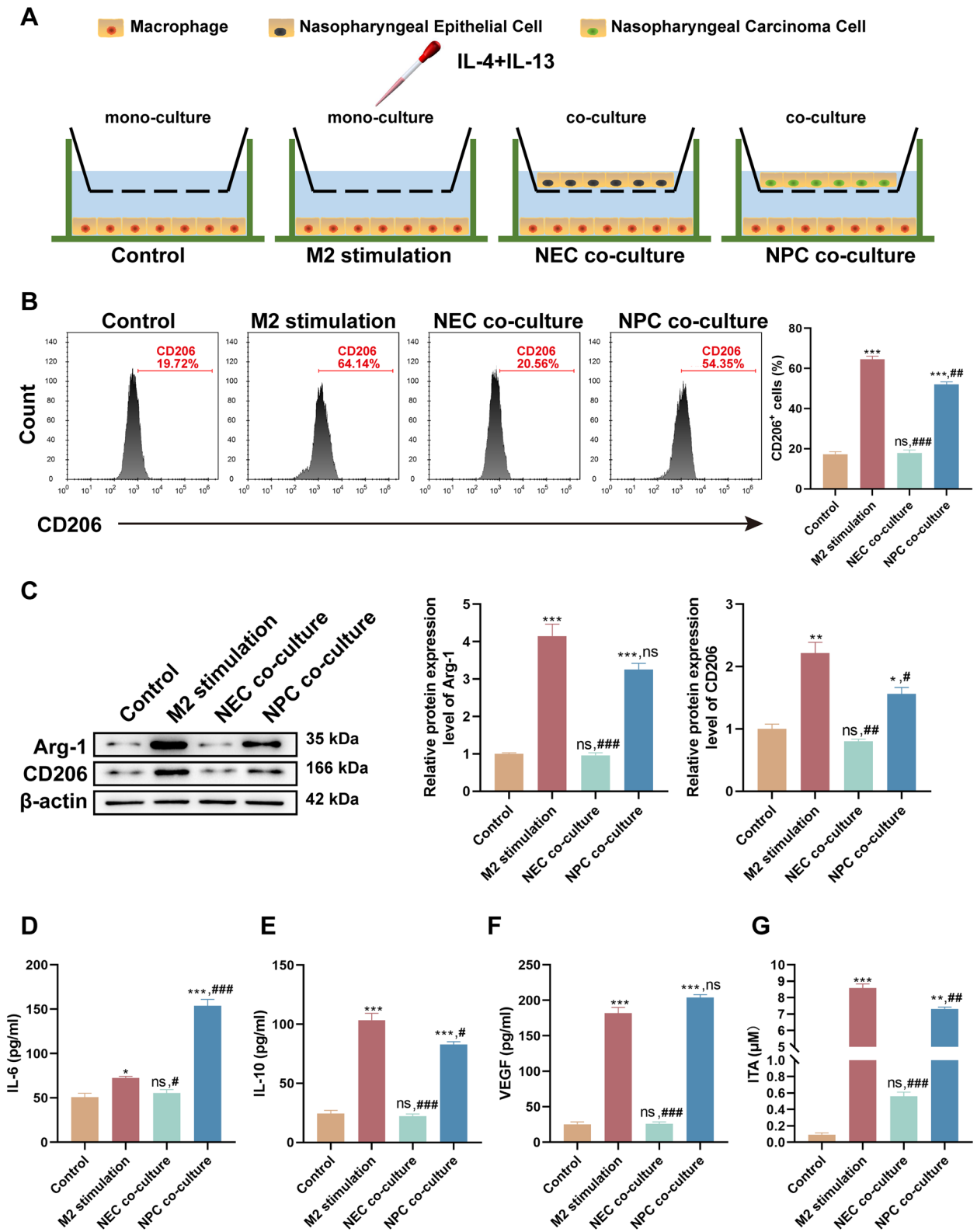
Zhang *et al. Cell Communication and Signaling*   (2024) 22:413

Page 5 of 18

Fig. 1 (See legend on previous page.)

Zhang *et al. Cell Communication and Signaling*   (2024) 22:413

Page 6 of 18

a 12-hour light/dark cycle, room temperature of 23 ± 2 °C, and humidity of 30–70%. All procedures were approved by the Laboratory Animal Welfare and Ethics Committee of the Third Xiangya Hospital, Central South University.

For subcutaneous xenograft experiments in huHSC-NCG mice, HK-1 cells (1×10^6 cells) were implanted in the right flank of huHSC-NCG mice. Fifteen days after the injection, huHSC-NCG mice were treated according to the following groupings: control (vehicle + isotype), ITA (ITA + isotype), anti-programmed cell death ligand-1 (PD-L1) (vehicle + anti-PD-L1), and ITA + anti-PD-L1 ($n = 6$ mice/group). Mice received intraperitoneal injections of vector/ITA and isotype/anti-PD-L1 treatments alternating daily. Mice were treated with 50 mg/kg ITA, and PBS was used as vehicle control. The isotype control (Catalog No. BE0089, Bioxcell) and anti-PD-L1 (Catalog No. BE0146 l, Bioxcell) were conducted (100 μg/mouse). For subcutaneous-tumor xenograft models in BALB/c mice, HK-1 cells (1×10^6 cells) were implanted in their right flank ($n = 6$ mice/group). Fifteen days after the injection, mice were treated based on the following groupings: control (vehicle) and ITA. Tumor sizes were measured every 4 days from day 12. Volume estimation was made according to the formula: $1/2 \times$ (length$\times$width^2). After 50 days of cells inoculation, all mice were sacrificed and tumor tissues were collected for further analysis.

Immunofluorescence (IF) assay
Tissue samples were blocked with 5% bovine serum albumin for 30 minutes at room temperature, followed by overnight incubation at 4°C with the primary antibody. The fluorescence-conjugated secondary antibody was then incubated for 1 hour at room temperature in the dark. The primary antibodies included anti-F4/80 (Catalog No. FNab02922, Fine Biotech Co., Ltd) and anti-CD163 (Catalog No. A72933, EpiGentek, USA) antibodies. Visualization of cell nuclei was performed using 4'-6-diamidino-2-phenylindole(Beyotime). Confocal microscope (LSM710, Zeiss, Jena, Germany) was utilized for the acquisition of fluorescence images.

Immunohistochemistry (IHC)
Paraffin-embedded slides were deparaffinized, rehydrated and then subjected to antigen retrieval. Endogenous peroxidase was then executed using 3% H_2O_2 solution. Following blocking with 10% goat serum, the tissues were incubated with a primary antibody against CD8 (Catalog No. LS-C414175, LSBio, USA) at 4°C overnight. After incubation with a biotin-conjugated secondary antibody, the immunoreactive protein was detected by 3,3'-diaminobenzidine staining. Images of representative areas were taken using a microscope.

Dot-blot assay
M0-type Mφs were treated with low, medium, and high concentrations of ITA, respectively. The collected cells were subjected to genomic DNA extraction by a genomic DNA purification kit (Catalog No. K0512, Thermo). The extracted DNA (1 μg) was mixed with $6 \times$ SSC (200 μL), followed by denaturation at 100 °C for 10 min. Spots were transferred to nitrocellulose membranes and dried. 5hmC (Catalog No. 39769, Active Motif, Carlsbad, CA) levels in cells were analyzed using standard protein blot analysis.

Statistical analysis
Statistical analyses were performed using GraphPad Prism software. Generally, a two-tailed *t*-test was utilized for the comparison of between 2 groups, and a one-way analysis of variance with Tukey's post hoc test was used for multiple comparisons. The data from at least triplicate independent experiments are are expressed as standard error of the mean (SEM). $P < 0.05$ was considered statistically significant.

Results
NPC cells evoked M2-type Mφ polarization and promoted ITA release from Mφs
To explore the crosstalk between NPC cells and TAMs, we co-cultured Mφs and HK-1 cells for 48 h. M2-type Mφs were induced by stimulation of THP-1 monocytes

(See figure on next page.)

Fig. 2 TAMs affected HK-1 cell malignant behaviors by regulating IRG1-mediated ITA production. (**A-F**) M2-type Mφs were used to imitate TAM models in vitro. **A** and **B** The knockdown efficiency of IRG1 in THP-1 monocytes by si-IRG1#1, si-IRG2#2 or si-IRG1#3 was verified by RT-qPCR and western blot. Data are expressed as means $\pm$ SEM and analyzed by one-way ANOVA (***$P < 0.001$, **$P < 0.01$, and *$P < 0.05$ vs. si-NC; ns, no significance). **C-D** The viability, colony formation, migration, and invasion of NPC cells in control (HK-1 cells stimulated with PBS), ITA (HK-1 cells stimulated with ITA), TAM-si-NC (HK-1 cells co-cultured with TAM-si-NC and stimulated with PBS), TAM-si-IRG1 (HK-1 cells co-cultured with TAM-si-IRG1 and stimulated with PBS), TAM-si-IRG1 + ITA (HK-1 cells co-cultured with TAM-si-IRG1 and stimulated with ITA) groups were estimated by CCK-8, colony formation, wound-healing, and transwell invasion assays. Data are expressed as means $\pm$ SEM and analyzed by one-way ANOVA (***$P < 0.001$, **$P < 0.01$, and *$P < 0.05$)
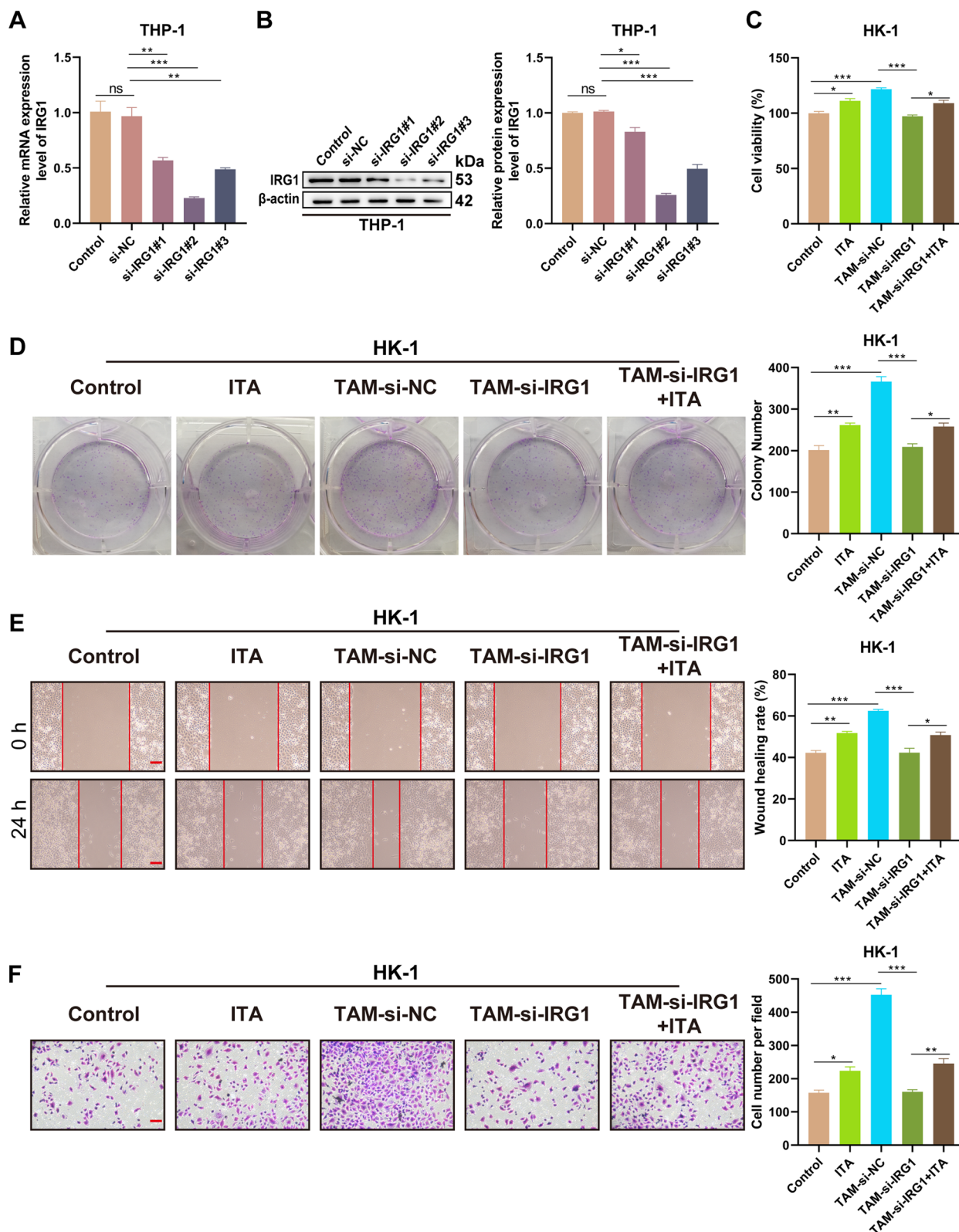
Fig. 2 (See legend on previous page.)

with IL-4 plus IL-13, as illustrated in Fig. 1A and B. Interestingly, co-culture with NPC cells resulted in a significant increase in the number of CD206$^+$ cells compared to mono-cultured THP-1 monocytes, but THP-1 monocytes co-cultured with NEC cells did not have these changes (Fig. 1A and B). As expected, protein levels of the M2-type markers Arg-1 and CD206 were significantly elevated after stimulation with IL-4 plus IL-13 or co-culture with NPC cells, whereas IL-4 plus IL-13 stimulation resulted in higher protein levels of Arg-1 and CD206 than co-culture with NPC cells (Fig. 1C). Similarly, the levels of cytokines IL-6, IL-10, and VEGF in supernatants derived from THP-1 monocytes stimulated with IL-4 plus IL-13 or co-cultured with NPC cells were higher compared to mono-cultured THP-1 monocytes (Fig. 1D-F). Because activated Mφs produce the unique small-molecule metabolite ITA that has a tumor-promoting effect, we measured the concentration of ITA in cell supernatants by GC-MS. The results showed that IL-4 plus IL-13 stimulation and co-culture with NPC cells caused an overt increase in the concentration of ITA relative to mono-cultured THP-1 monocytes. Collectively, these results manifested that HK-1 cells induced M2-type Mφ polarization and contributed to the release of ITA from Mφs.

TAMs facilitated NPC cell malignant behaviors by regulating IRG1-mediated ITA levels

Since TAMs and M2-type Mφs share significant phenotypic and functional similarities, M2-type Mφs with immunosuppressive specificity are frequently used as models to investigate the action of TAMs. Researchers have demonstrated that IRG1-encoded aconitate decarboxylase 1 catalyzes ITA production [16]. Therefore, we further investigated whether IRG1-mediated production of ITA in TAMs affects HK-1 cell malignant behaviors. The importance of IRG1-mediated production of ITA in TAMs was discussed by the loss-of-function strategy. The knockdown efficiency of each siRNA was validated by RT-qPCR and western blot, as exhibited in Fig. 2A and B. As a note, the si-IRG1#2 with the best knockdown efficiency was employed for subsequent functional validation. We discovered that both ITA and TAMs elevated

HK-1 cell viability and contributed to the colony formation, migrating, and invading capacities of HK-1 cells, whereas these effects mediated by TAMs were undercut upon IRG1 knockdown. Importantly, ITA partly overthrow the inhibiting effects of IRG1-knockdown TAMs on HK-1 cell proliferation, migration, and invasion (Fig. 2C-F). The above experiments were performed with the NPC cell line HNE2 for further validation. The same results were observed in HNE2 cells, that was, TAMs promoted colony formation, migration, and invasion of HNE2 cells by regulating IRG1-mediated ITA production (Supplementary Fig. 1A-C). Taken altogether, these outcomes manifested that TAMs regulated IRG1-mediated production of ITA to affect NPC cell malignant behaviors.

IRG1-mediated ITA regulated the M2-type polarization and phagocytosis of TAMs

Subsequently, we co-cultured M0-type Mφs and HK-1 cells to analyze the influence of ITA on the M2-type polarization of TAMs. In terms of CD206$^+$ TAMs, the percentage of CD206$^+$ TAMs was higher in the TAM-si-NC group compared with the control group (M0-type), but IRG1 silencing decreased the percentage of CD206$^+$ TAMs. Also, IRG1 silencing-mediated decrease in the percentage of CD206$^+$ TAMs was overthrown after ITA supplementation (Fig. 3A). Moreover, the levels of IL-6, IL-10, and VEGF released from TAMs were markedly elevated after co-culture with HK-1 cells. Under the same culture conditions, knockdown of IRG1 in TAMs reversed the increase in cytokine levels described above, while IRG1 inhibition-mediated effects were eliminated following ITA addition (Fig. 3B-D). Next, we analyzed the phagocytic function of TAMs. Treated TAMs were co-cultured with new HK-1 cells labeled with mitoTracker deep red. Flow cytometry results showed that phagocytosis of TAMs was inhibited after co-culture with HK-1 cells, but the above-constrained phagocytosis was restored after IRG1 knockdown. As expected, IRG1 knockdown-mediated effects on the improvement of phagocytosis of TAMs were overridden after ITA addition (Fig. 3E). The above results regarding the effect of ITA on the M2-type

(See figure on next page.)

Fig. 3 IRG1-mediated ITA promoted the M2-type polarization and decreased the phagocytosis of TAMs. **A** Flow cytometry analysis of the percentage of CD206$^+$ TAMs in control (M0-type Mφs), TAM-si-NC (PBS-treated HK-1 cells co-cultured with TAM-si-NC), TAM-si-IRG1 (PBS-treated HK-1 cells co-cultured with TAM-si-IRG1), and TAM-si-IRG1 + ITA (ITA-treated HK-1 cells co-cultured with TAM-si-IRG1) groups. **B-D** ELISA detection of the levels of IL-6, IL-10, and VEGF released from TAMs. **E** Flow cytometry determination of the phagocytosis of treated TAMs for re-co-cultured HK-1 cells. **F** Flow cytometry analysis of the percentage of CD206$^+$ TAMs in control (M0-type Mφs), TAM-si-NC (HNE2 cells co-cultured with TAM-si-NC + PBS), TAM-si-IRG1 (HNE2 cells co-cultured with TAM-si-IRG1 + PBS), and TAM-si-IRG1 + ITA (HNE2 cells co-cultured with TAM-si-IRG1 + ITA) groups. **G-I** The levels of IL-6, IL-10, and VEGF released from TAMs were measured. **J** Flow cytometry determination of the phagocytosis of treated TAMs. Data are expressed as means ± SEM and analyzed by one-way ANOVA (***$P < 0.001$, **$P < 0.01$, and *$P < 0.05$)
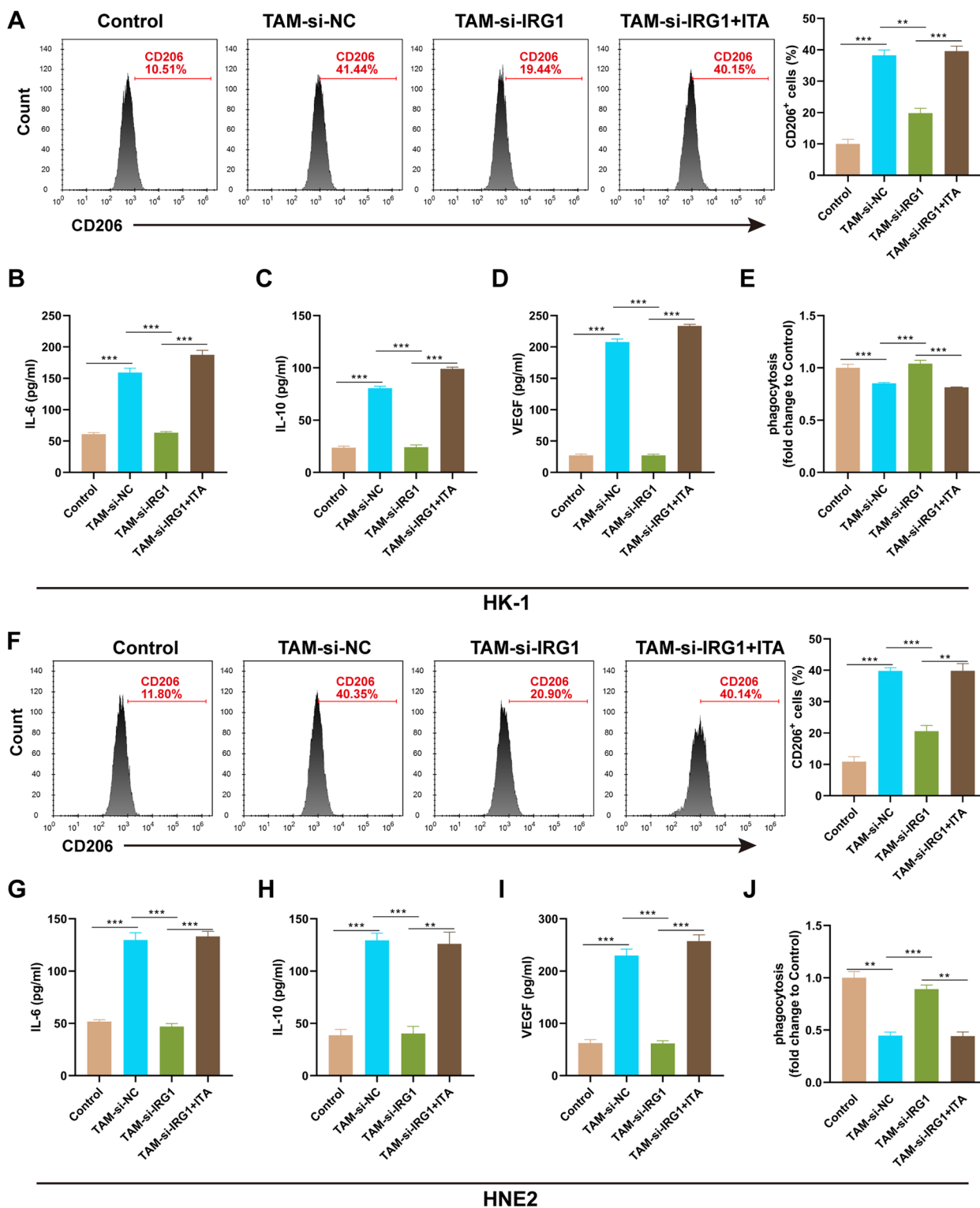
Fig. 3 (See legend on previous page.)

polarization and phagocytic capacity of TAMs were subsequently confirmed by co-culturing M0-type Mϕs with HNE2 cells. Consistently, we observed that IRG1

knockdown-mediated inhibition in M2-type polarization and promotion in phagocytic capacity of TAMs were restored upon the addition of ITA (Fig. 3F-J). All

results manifested that IRG1-mediated ITA facilitated the M2-type polarization of TAMs and restrained the phagocytosis of TAMs.

IRG1-mediated ITA decreased the killing of CD8+ T cells

To estimate the function of ITA on cytotoxic T cell killing, we isolated CD8$^+$ T cells from the spleens of OT-1 mice and co-cultured them with SIINFEKL-presenting HK-1 cells by CM from different culture systems. The results showed that incubation with CM from the ITA group did not affect the apoptosis of SIINFEKL-presenting HK-1 cells co-cultured with CD8$^+$ T cells compared with their incubation with CM from the control group. However, an overt reduction was observed after incubation with CM from the TAM-si-NC group, whereas this decreased apoptotic rate was reversed following IRG1 knockdown. Importantly, the influence mediated by IRG1 knockdown was overturned after ITA addition (Fig. 4A). Furthermore, the fluorescence intensity in the cell supernatants of HK-1 cells with luciferase genes in the ITA group did not change differentially versus the control group. However, the fluorescence intensity in the cell supernatants of HK-1 cells in the TAM-si-NC group was lower in comparison with the control group, but the reduced fluorescence intensity was restored after IRG1 knockdown. Interestingly, ITA supplementation eliminated the IRG1 knockdown-mediated effects (Fig. 4B). We also detected the release of INF-γ from CD8$^+$ T cells. As shown in Fig. 4C, the trend variations in the concentration of INF-γ in the different groups were consistent with the apoptotic status of the HK-1 cells and the lysis of HK-1 cells transfected with fluorescent genes. We subsequently validated the above results with the NPC cell line HNE2. Figure 4D-F showed that IRG1-mediated ITA restrained the cytotoxicity of CD8$^+$ T cells toward HNE2 cells. These results clustered together suggested that IRG1-mediated ITA suppressed the cytotoxicity of CD8$^+$ T cells toward NPCs.

ITA exerted a tumor-promoting role in NPC by mediating immune escape

After determining the promoting effect of ITA on the malignant behaviors of NPC cells in vitro, we explored the effect of the combination of ITA with an anti-PD-1 antibody on the growth of subcutaneous xenograft tumors in CD34$^+$ hematopoietic stem cell humanized mice (Fig. 5A). The results exhibited that ITA treatment resulted in a larger tumor volume. On the contrary, administration of an anti-PD-L1 antibody had an inhibitory effect on tumor growth. However, tumors derived from the ITA + anti-PD-L1 antibody group were smaller than the ITA group but larger than the anti-PD-1 antibody group (Fig. 5B and C). IF detection of M2-type TAMs in tumor tissues showed that the ITA group had the highest number of M2-type TAMs, followed by the ITA + anti-PD-L1 and control groups that had little difference in the number of M2-type TAMs. As expected, the anti-PD-L1 group had the lowest number of M2-type TAMs (Fig. 5D). The reversal of the above order was the trend in the number of M1-type TAMs (Fig. 5D). In addition, the ranking of the percentage of CD8$^+$T-positive in tumor tissues in the above subgroups was as follows: ITA < control < ITA + anti-PD-L1 < anti-PD-L1 (Fig. 5E). We further verified whether ITA exerts pro-cancer effects through the immune system by administering ITA to BALB/c nude mice (Fig. 6A). The outcomes exhibited that administering ITA did not result in a marked alteration in tumor volume of immune-deficient BALB/c mice compared with the control group (Fig. 6B and C). These results manifested that ITA played a pro-cancer role in NPC by promoting tumor immune escape.

ITA played a tumor immunosuppressive role by dampening TET2 expression

Given that ITA can attenuate the pro-inflammatory response of Mφs by inhibiting TET2 [17], we next further explored whether TET2 is regulated by ITA in the pro-carcinogenic effects of NPC. Based on the fact that TET2 is a DNA demethylase that promotes tumor

(See figure on next page.)

Fig. 4 IRG1-mediated ITA repressed the killing of CD8$^+$T cells. CD8$^+$ T cells were isolated from the spleens of OT-1 mice and co-cultured with SIINFEKL-presenting NPC cells in CM. **A** Flow cytometry analysis of the apoptosis of SIINFEKL-presenting HK-1 cells in control (HK-1 cells treated with PBS), ITA (HK-1 cells stimulated with ITA), TAM-si-NC (PBS-treated HK-1 cells co-cultured with TAM-si-NC), TAM-si-IRG1 (PBS-treated HK-1 cells co-cultured with TAM-si-IRG1), and TAM-si-IRG1 + ITA (ITA-stimulated HK-1 cells co-cultured with TAM-si-IRG1) groups. **B** The percentage of lysed SIINFEKL-presenting HK-1 cells with luciferase genes was assessed depending on the fluorescence intensity. **C** ELISA measurement of the levels of INF-γ released from CD8$^+$ T cells. **D** Flow cytometry analysis of the apoptosis of SIINFEKL-presenting HNE2 cells co-cultured with CD8$^+$ T cells in control (HNE2 cells stimulated with PBS), ITA (HNE2 cells stimulated with ITA), TAM-si-NC (PBS-treated HNE2 cells co-cultured with TAM-si-NC), TAM-si-IRG1 (PBS-treated HNE2 cells co-cultured with TAM-si-IRG1), and TAM-si-IRG1 + ITA (ITA-treated HNE2 cells co-cultured with TAM-si-IRG1) groups. **E** Assessment of the percentage of lysed HNE2 cells containing the luciferase gene was performed by analyzing the fluorescence intensity. **F** ELISA measurement of the levels of INF-γ released from CD8$^+$ T cells. Data are expressed as means ± SEM and analyzed by one-way ANOVA (***$P < 0.001$, **$P < 0.01$, and *$P < 0.05$)

Zhang *et al. Cell Communication and Signaling*   (2024) 22:413
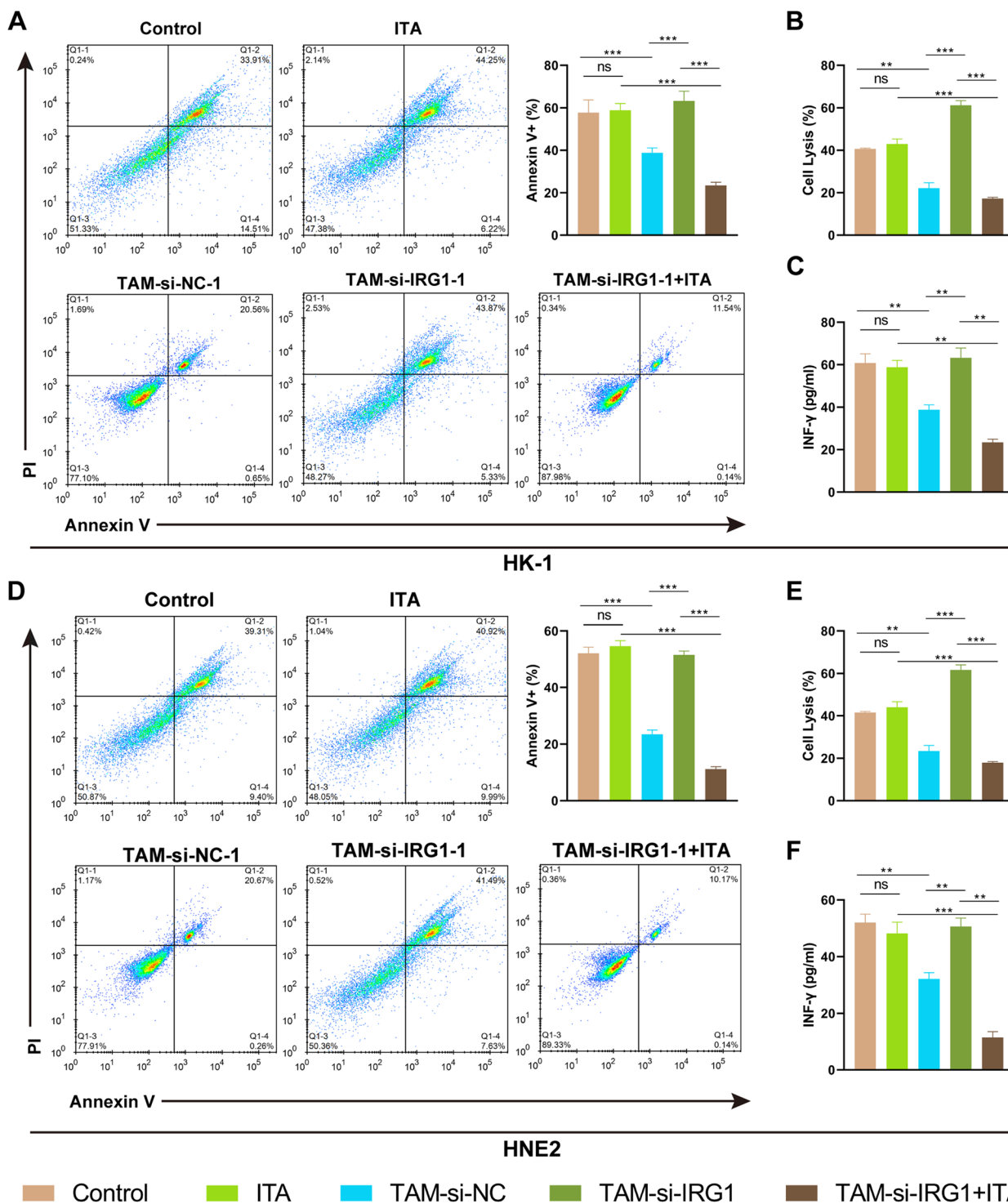
Page 11 of 18

Fig. 4 (See legend on previous page.)

immunity and improves the efficiency of immunotherapy, we first detected the effect of ITA on 5hmC levels in M0-type Mφs. Dot blot images displayed that 5hmC

levels were inhibited by ITA in a dose-dependent manner (Fig. 7A). To investigate whether TET2 takes part in the pro-carcinogenic effects of ITA, we knocked down TET2

in THP-1 monocytes. A significant reduction in TET2 mRNA and protein levels was observed in THP-1 monocytes following si-TET2#1, si-TET2#2, or si-TET2#3 transfection (Fig. 7B and C). Furthermore, ITA promoted M2-type TAM polarization, but TET2 knockdown repressed M2-type TAM polarization, however, the co-action of TET2 knockdown and ITA elevated M2-type TAM polarization relative to TET2 knockdown alone, manifesting that ITA not only acts with TET2 but also participates in M2-type TAM polarization through other pathways (Fig. 7D). Moreover, ITA stimulation increased the levels of IL-6, IL-10, and VEGF in M0-type TAM Mφs, yet ITA did not affect the levels of these cytokines in TET2-knockdown M0-type TAM Mφs (Fig. 7E-G). Furthermore, we further analyzed whether ITA mediates the phagocytosis of TAMs and the killing function of CD8$^+$T cells via TET2. ITA decreased the phagocytosis of TAMs, but it had little effect on TAM phagocytosis in the presence of TET2 knockdown (Fig. 7H). In addition, the apoptosis of HK-1 cells co-cultured with CD8$^+$T cells was weakened after incubation with CM from the ITA and si-TET2 groups. Moreover, differential changes in HK-1 cell apoptosis in the si-TET2 and si-TET2 + ITA groups were not significant (Fig. 7I). Also, incubation with CM from the ITA and si-TET2 groups decreased CD8$^+$T cell killing and the release of INF-γ. However, there was no significant change in CD8$^+$T cell killing and INF-γ release in the si-TET2 group compared to the si-TET2 + ITA group (Fig. 7J and K). Collectively, ITA played a tumor immunosuppressive role via TET2.

Discussion

As the major infiltrating cell sub-population in TME, the significant role of TAMs in tumor progression has attracted great attention [18]. Recently, a variety of immunotherapies targeting TAMs have brought benefits to tumor patients, but they also have certain limitations, such as poor compatibility with other immunotherapies [19, 20]. Therefore, exploring the molecular mechanisms associated with TAMs is crucial for the development of new immunotherapeutic strategies for NPC. This study uncovered that TAM-derived ITA impaired the killing of CD8$^+$ T cells and decreased phagocytosis of TAMs via TET2, thus promoting NPC cell proliferation, migration, and invasion (Fig. 8).

Since the functional and phenotypic characteristics of TAMs are closer to those of M2-type Mφs, TAMs mainly refer to M2-type Mφs rather than M1-type Mφs [21]. The recruitment and functional polarization of TAMs in the TME is an extremely complex process that is regulated by various cytokines and environmental factors [22]. Tumor cells can recruit circulating monocytes and enhance their ability to polarize toward M2-type TAMs [23]. ITA is a metabolic product of Mφs, it has been revealed to play different roles in different diseases by promoting M2-type Mφ polarization [24–26]. Ni et al. reported that ITA inhibits extracellular matrix degeneration and inflammation in mouse osteoarthritis models by facilitating M2-type Mφ polarization, thus lessening osteoarthritis [25]. Here, we identified that HK-1 cells can induce M2-type polarization of M0-type Mφs as well as promote ITA release from Mφs, suggesting that HK-1 cells may promote M2-type Mφ polarization by inducing ITA production.

IRG1-mediated production and accumulation of ITA is an important negative regulatory point in the modulation of Mφ inflammation, which inhibits the inflammatory response and regulates disease progression through multiple mechanisms [27, 28]. Recent studies have found that IRG1-induced ITA inhibits succinate dehydrogenase (SDH) expression and activity, thereby blocking succinate-mediated inflammatory responses [29] and preventing reverse electron transfer-generated reactive oxygen species to decrease inflammatory responses [30]. In tumors, inactivation of SDH and fenugreek hydratase causes accumulation of succinate and fenugreek in the cytosol, leading to inhibition of the proline hydroxylase family, thereby enhancing tumor cell glycolysis and making cells resistant to apoptotic signals [31]. Furthermore, targeting IRG1 can revert TAM-mediated immunosuppression and augment immunotherapy for cancer [16]. Also, ITA derived from myeloids facilitates tumor growth through repressing the cytotoxicity of CD8$^+$T cells [11]. Herein, ITA addition weakened the inhibitory effects of IRG1-knockdown TAMs on NPC cell proliferation, migration, and invasion. Also, the promoting effects of IRG1-knockdown TAMs on the cytotoxicity of CD8$^+$T cells and the decreased M2-type TAM polarization of IRG1-knockdown TAMs and the elevated phagocytosis of IRG1-knockdown TAMs were reversed after ITA

(See figure on next page.)
Fig. 5 ITA promoted the growth of subcutaneous xenograft tumors by mediating immune escape. **A** Schematic diagram of animal experiments (CD34$^+$ hematopoietic stem cell humanized mice) (*n* = 6). **B** The growth curves of subcutaneous xenograft tumors. **C** Photographs of the subcutaneous tumors. **D** IF analysis of the percentage of infiltrated F4/80 $^+$ Mφs and CD163$^+$ Mφs in subcutaneous xenograft tumors. **E** IHC assessment of the expression of CD8 in subcutaneous xenograft tumors. Data are expressed as means ± SEM and analyzed by one-way ANOVA (***P < 0.001, **P < 0.01, and *P < 0.05)
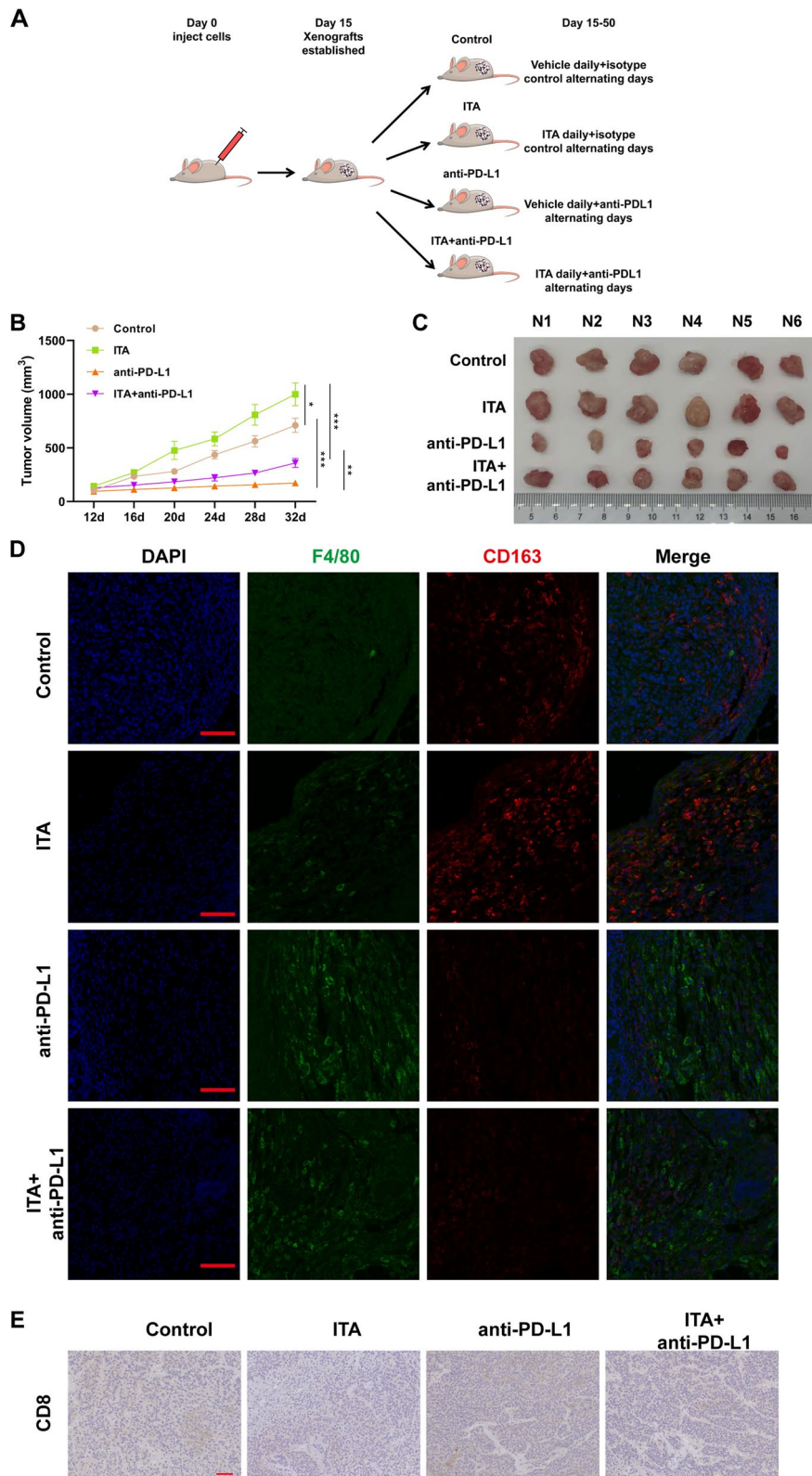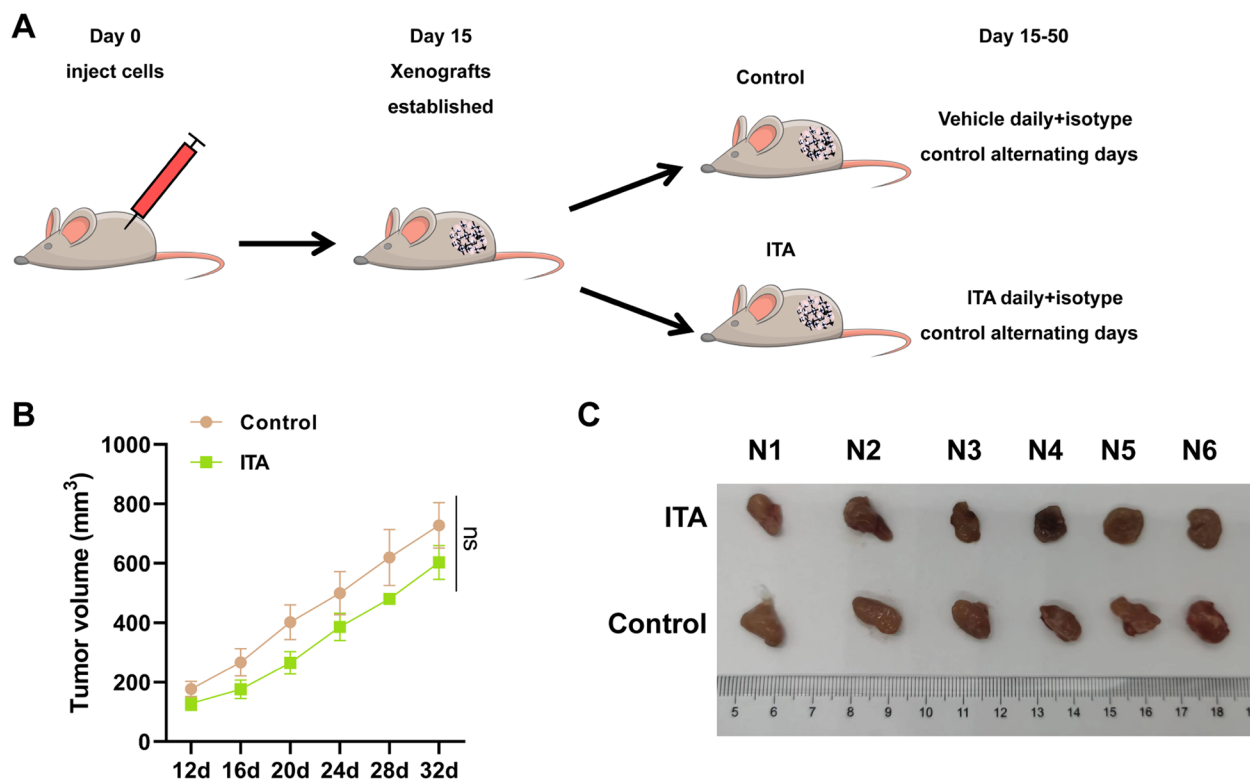
Fig. 5 (See legend on previous page.)

Fig. 6 The pro-carcinogenic effects of ITA were attenuated in nude mice lacking an immune system. **A** Tumor growth of HK-1 cell-bearing BALB/c nude mice (*n*=6). **B** The tumor growth curve of subcutaneous NPC. **C** Typical animal in vivo imaging pictures. Data are expressed as means±SEM and analyzed by unpaired t-test (*P<0.05)

addition. Furthermore, ITA promoted the growth of subcutaneous xenograft tumors and enhanced M2-type TAM polarization in CD34$^+$ hematopoietic stem cell humanized mice, but the anti-PD-L1 antibody had the opposite effect. However, the tumor-promoting of ITA was impaired after administration with anti-PD-L1 antibody. Notably, administration of ITA did not result in significant changes in tumor volume of immune-deficient BALB/c mice compared to the control group. Similarly, several studies suggested that elements that depend on immune escape to work, play little role in immune-deficient mice [32–34]. These results manifested that ITA

facilitates tumor growth by fostering immune escape under immuno-normal conditions.

TET2 is a member of the TET gene family, and TET2 catalyzes the conversion of 5mC to 5hmC in DNA, resulting in DNA demethylation [35]. TET2, a potential tumor-repressive gene, is involved in the epigenetic regulation of methylation or demethylation of early hematopoietic-related genes [36]. Mutation or knockdown of TET2 drives tumorigenesis in several hematological and solid cancers, such as renal cell carcinoma [37] and acute myeloid leukemia [38]. A recent study showed that ITA can interact with TET2 to suppress lipopolysaccharide -induced gene expression in Mφs by binding to and inhibiting TET2

(See figure on next page.)
Fig. 7 ITA played a tumor immunosuppressive role by interacting with TET2. **A** Dot blot images showed 5hmC levels in M0-type Mφs treated with different concentrations of ITA. **B** and **C** Validation of the interference efficiency of si-TET2#1, si-TET2#2, and si-TET2#3 on TET2 in THP-1 monocytes. **D** Measurement of the percentage of CD206$^+$ TAMs in control (PBS-treated HK-1 cells co-cultured with TAM-si-NC), ITA (ITA-treated HK-1 cells co-cultured with TAM-si-NC), si-TET2 (PBS-treated HK-1 cells co-cultured with TAM-si-TET2), and si-TET2 + ITA (ITA-treated HK-1 cells co-cultured with TAM-si-TET2) groups. **E**-**G** Analysis of the levels of IL-6, IL-10, and VEGF released from TAMs at different groups. **H** The phagocytosis of TAMs was determined by flow cytometry. **I** Effect of CD8$^+$T cells on HK-1 cell apoptosis. **J** The killing of CD8$^+$T cells was determined by the assessment of fluorescence intensity. **K** The release of INF-γ from CD8$^+$ T cells. Data are expressed as means±SEM and analyzed by one-way ANOVA (***P<0.001, **P<0.01, and *P<0.05)
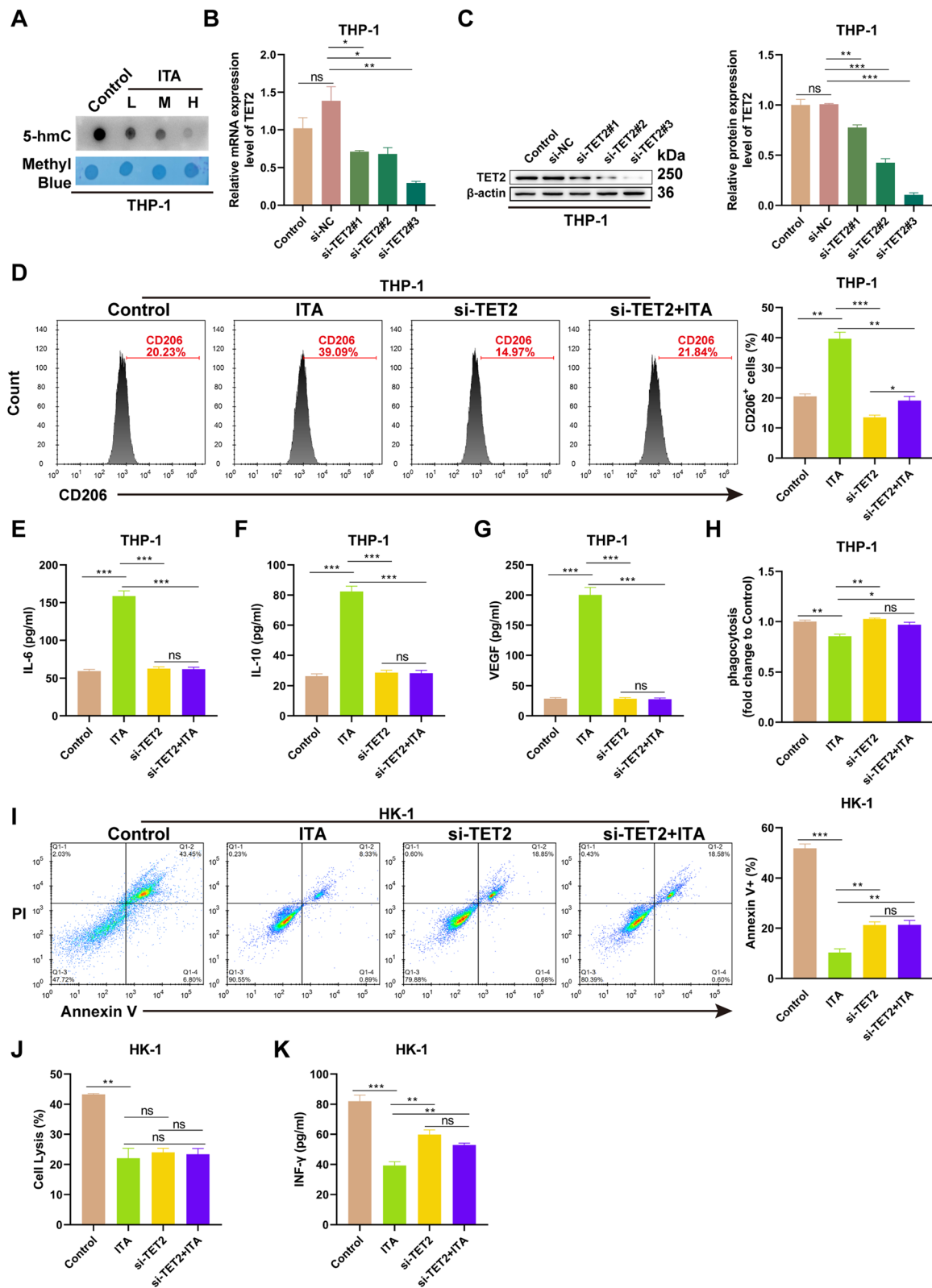
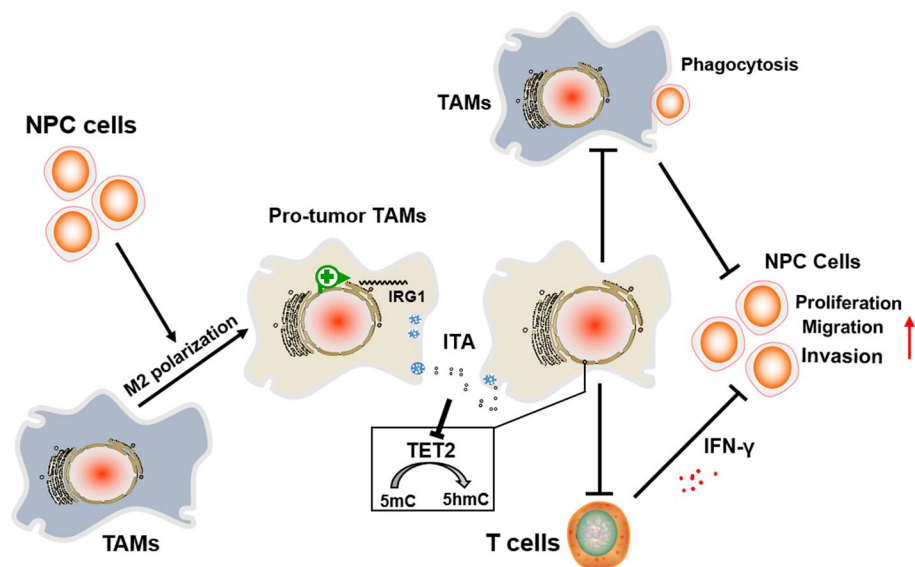**Fig. 7** (See legend on previous page.)

Fig. 8 A schematic diagram showing that Tumor-associated macrophage-derived itaconic acid contributes to nasopharyngeal carcinoma progression by promoting immune escape via TET2 NPC cells promoted the M2-type polarization of TAMs and IRG1-mediated release of ITA from TAMs. and then weakened the killing of CD8+ T cells and reduced the phagocytosis of TAMs by interacting with TET2, thereby promoting the proliferation, migration, and invasion of NPC cells

expression [17]. Here, the levels of 5hmC were repressed in M0-type Mφs by ITA in a dose-dependent manner, implying that ITA suppresses the expression of TET2. Furthermore, ITA promoted M2-type TAM polarization, repressed the phagocytosis of TAMs, reduced the killing of CD8+ T cells, but had little effect on the above metrics after TET2 knockdown, manifesting that ITA played a tumor-promoting action by repressing TET2 expression. Additionally, ITA exerts its effects not only through TET2, and the mechanism by which ITA works through other targets needs to be further explored. Unfortunately, we have not performed associated assays with clinical samples, which is a direction for future exploration.

In conclusion, TAMs-derived ITA promotes NPC progression by facilitating immune escape by inhibiting TET2 expression, indicating that targeting the metabolic pathways that produce ITA may be a possible means of interfering with this tumor.

Abbreviations

NPC	Nasopharyngeal carcinoma
ITA	Itaconic acid
TAM	Tumor-associated macrophage
Mφs	Macrophages
IRG1	Immune-responsive gene
TET2	Tet methylcytosine dioxygenase 2
TME	Tumor microenvironment
CTLs	Cytotoxic T lymphocytes
NECs	Nasopharyngeal epithelial cells
P/S	Penicillin-streptomycin
RT-qPCR	Reverse transcription-quantitative PCR
CM	Conditioned medium
IFN-γ	Interferon-gamma
PD-L1	Programmed cell death ligand-1
IF	Immunofluorescence
ELISA	Enzyme-linked immunosorbent assay
IHC	Immunohistochemistry
SEM	Standard error of the mean

Supplementary Information

The online version contains supplementary material available at https://doi.org/10.1186/s12964-024-01799-0.

Supplementary Material 1. Supplementary Fig. 1 IRG1-mediated ITA facilitated HNE2 cell malignant behaviors. (A-C) The colony formation, migration, and invasion of NPC cells in control (HNE2 cells stimulated with PBS), ITA (HNE2 cells stimulated with ITA), TAM-si-NC (PBS-treated HNE2 cells co-cultured with TAM-si-NC), TAM-si-IRG1 (PBS-treated HNE2 cells co-cultured with TAM-si-IRG1), and TAM-si-IRG1+ITA (ITA-treated HNE2 cells co-cultured with TAM-si-IRG1) groups. Data are expressed as means ± SEM and analyzed by one-way ANOVA (***$P < 0.001$, **$P < 0.01$, and *$P < 0.05$).

Supplementary Material 2. Supplementary Fig. 2. Flow cytometry plots to reveal the phagocytosis of treated TAMs of Figure 3E and 3G. (A) The phagocytosis percentage of treated TAMs in HK-1. (B) The phagocytosis percentage of treated TAMs in HNE-2.

Authors' contributions
The concept and design of the present study were provided by ZX. XZ and SQ performed the research and the data analysis. Experiment data were collected and analyzed by PW, BY, DY , XP and ZX. XZ, SQ and ZX produced and revised the manuscript. ZX and SL conducted data auditing and manuscript review. All authors read and approved the final manuscript.

Availability of data and materials
No datasets were generated or analysed during the current study.

Declarations

Ethical approval and consent to participate
All protocols were reviewed and approved by the Joint Ethics Committee of the Third Xiangya Hospital, the Central South University Health Authority and performed in accordance with national guidelines.

Consent for publication
This manuscript has been read and approved by all the authors to publish and is not submitted or under consideration for publication elsewhere.

Competing interests
The authors declare no competing interests.

References
1. Bossi P, Chan AT, Licitra L, Trama A, Orlandi E, Hui EP, et al. Nasopharyngeal carcinoma: ESMO-EURACAN clinical practice guidelines for diagnosis, treatment and follow-up(†). Ann Oncol. 2021;32(4):452–65.
2. Chiang CL, Guo Q, Ng WT, Lin S, Ma TSW, Xu Z, et al. Prognostic factors for overall survival in nasopharyngeal Cancer and implication for TNM staging by UICC: a systematic review of the literature. Front Oncol. 2021;11:703995.
3. de Visser KE, Joyce JA. The evolving tumor microenvironment: from cancer initiation to metastatic outgrowth. Cancer Cell. 2023;41(3):374–403.
4. Joyce JA, Fearon DT. T cell exclusion, immune privilege, and the tumor microenvironment. Science. 2015;348(6230):74–80.
5. Xiang X, Wang J, Lu D, Xu X. Targeting tumor-associated macrophages to synergize tumor immunotherapy. Signal Transduct Target Ther. 2021;6(1):75.
6. Pan Y, Yu Y, Wang X, Zhang T. Tumor-Associated macrophages in Tumor Immunity. Front Immunol. 2020;11:583084.
7. Wei YT, Wang XR, Yan C, Huang F, Zhang Y, Liu X, et al. Thymosin α-1 reverses M2 polarization of Tumor-Associated macrophages during Efferocytosis. Cancer Res. 2022;82(10):1991–2002.
8. Lafta HA, AbdulHussein AH, Al-Shalah SAJ, Alnassar YS, Mohammed NM, Akram SM, et al. Tumor-associated macrophages (TAMs) in Cancer Resistance; modulation by Natural products. Curr Top Med Chem. 2023;23(12):1104–22.
9. Wu K, Lin K, Li X, Yuan X, Xu P, Ni P, et al. Redefining Tumor-Associated macrophage subpopulations and functions in the Tumor Microenvironment. Front Immunol. 2020;11:1731.
10. Michelucci A, Cordes T, Ghelfi J, Pailot A, Reiling N, Goldmann O, et al. Immune-responsive gene 1 protein links metabolism to immunity by catalyzing itaconic acid production. Proc Natl Acad Sci U S A. 2013;110(19):7820–5.
11. Zhao H, Teng D, Yang L, Xu X, Chen J, Jiang T, et al. Myeloid-derived itaconate suppresses cytotoxic CD8(+) T cells and promotes tumour growth. Nat Metab. 2022;4(12):1660–73.
12. Gu X, Wei H, Suo C, Shen S, Zhu C, Chen L, et al. Itaconate promotes hepatocellular carcinoma progression by epigenetic induction of CD8(+) T-cell exhaustion. Nat Commun. 2023;14(1):8154.
13. Weiss JM, Davies LC, Karwan M, Ileva L, Ozaki MK, Cheng RY, et al. Itaconic acid mediates crosstalk between macrophage metabolism and peritoneal tumors. J Clin Invest. 2018;128(9):3794–805.
14. Meiser J, Kraemer L, Jaeger C, Madry H, Link A, Lepper PM, et al. Itaconic acid indicates cellular but not systemic immune system activation. Oncotarget. 2018;9(63):32098–107.
15. Livak KJ, Schmittgen TD. Analysis of relative gene expression data using real-time quantitative PCR and the 2(-Delta Delta C(T)) method. Methods. 2001;25(4):402–8.
16. Chen YJ, Li GN, Li XJ, Wei LX, Fu MJ, Cheng ZL, et al. Targeting IRG1 reverses the immunosuppressive function of tumor-associated macrophages and enhances cancer immunotherapy. Sci Adv. 2023;9(17):eadg0654.
17. Chen LL, Morcelle C, Cheng ZL, Chen X, Xu Y, Gao Y, et al. Itaconate inhibits TET DNA dioxygenases to dampen inflammatory responses. Nat Cell Biol. 2022;24(3):353–63.
18. Christofides A, Strauss L, Yeo A, Cao C, Charest A, Boussiotis VA. The complex role of tumor-infiltrating macrophages. Nat Immunol. 2022;23(8):1148–56.
19. Barth ND, Van Dalen FJ, Karmakar U, Bertolini M, Mendive-Tapia L, Kitamura T, et al. Enzyme-activatable chemokine conjugates for in vivo targeting of Tumor-Associated macrophages. Angew Chem Int Ed Engl. 2022;61(41):e202207508.
20. Zhang L, Lin Y, Li S, Guan X, Jiang X. In situ reprogramming of Tumor-Associated macrophages with internally and externally Engineered exosomes. Angew Chem Int Ed Engl. 2023;62(11):e202217089.
21. Li H, Somiya M, Kuroda S. Enhancing antibody-dependent cellular phagocytosis by re-education of tumor-associated macrophages with resiquimod-encapsulated liposomes. Biomaterials. 2021;268:120601.
22. Boutilier AJ, Elsawa SF. Macrophage polarization States in the Tumor Microenvironment. Int J Mol Sci 2021; 22(13).
23. Patysheva M, Frolova A, Larionova I, Afanas'ev S, Tarasova A, Cherdyntseva N, et al. Monocyte programming by cancer therapy. Front Immunol. 2022;13:994319.
24. Ganta VC, Choi MH, Kutateladze A, Fox TE, Farber CR, Annex BH. A MicroRNA93-Interferon Regulatory factor-9-Immunoresponsive gene-1-Itaconic acid pathway modulates M2-Like Macrophage polarization to Revascularize ischemic muscle. Circulation. 2017;135(24):2403–25.
25. Ni L, Lin Z, Hu S, Shi Y, Jiang Z, Zhao J, et al. Itaconate attenuates osteoarthritis by inhibiting STING/NF-κB axis in chondrocytes and promoting M2 polarization in macrophages. Biochem Pharmacol. 2022;198:114935.
26. Xiao H, Dong Y, Wan D, Wan J, Huang J, Tang L, et al. Injectable hydrogel loaded with 4-octyl itaconate enhances cartilage regeneration by regulating macrophage polarization. Biomater Sci. 2023;11(7):2445–60.
27. Duan X, Hu M, Yang L, Zhang S, Wang B, Li T, et al. IRG1 prevents excessive inflammatory responses and cardiac dysfunction after myocardial injury. Biochem Pharmacol. 2023;213:115614.
28. Li W, Li Y, Kang J, Jiang H, Gong W, Chen L, et al. 4-octyl itaconate as a metabolite derivative inhibits inflammation via alkylation of STING. Cell Rep. 2023;42(3):112145.
29. O'Neill LAJ, Artyomov MN. Itaconate: the poster child of metabolic reprogramming in macrophage function. Nat Rev Immunol. 2019;19(5):273–81.
30. Luan HH, Medzhitov R. Food Fight: role of Itaconate and other metabolites in Antimicrobial Defense. Cell Metab. 2016;24(3):379–87.
31. King A, Selak MA, Gottlieb E. Succinate dehydrogenase and fumarate hydratase: linking mitochondrial dysfunction and cancer. Oncogene. 2006;25(34):4675–82.
32. Zeng Q, Saghafinia S, Chryplewicz A, Fournier N, Christe L, Xie YQ, et al. Aberrant hyperexpression of the RNA binding protein FMRP in tumors mediates immune evasion. Science. 2022;378(6621):eabl7207.
33. Lee CH, Bae JH, Choe EJ, Park JM, Park SS, Cho HJ, et al. Macitentan improves antitumor immune responses by inhibiting the secretion of tumor-derived extracellular vesicle PD-L1. Theranostics. 2022;12(5):1971–87.
34. Sun P, Zhang X, Wang RJ, Ma QY, Xu L, Wang Y et al. PI3Kα inhibitor CYH33 triggers antitumor immunity in murine breast cancer by activating CD8(+)T cells and promoting fatty acid metabolism. J Immunother Cancer. 2021;9(8):e003093.
35. Jiang S. Tet2 at the interface between cancer and immunity. Commun Biol. 2020;3(1):667.
36. Chiba S. Dysregulation of TET2 in hematologic malignancies. Int J Hematol. 2017;105(1):17–22.

Zhang *et al. Cell Communication and Signaling*   (2024) 22:413

Page 18 of 18

37. Zhang X, Li S, He J, Jin Y, Zhang R, Dong W, et al. TET2 suppresses VHL Deficiency-Driven Clear Cell Renal Cell Carcinoma by inhibiting HIF Signaling. Cancer Res. 2022;82(11):2097–109.
38. Li Y, Xue M, Deng X, Dong L, Nguyen LXT, Ren L, et al. TET2-mediated mRNA demethylation regulates leukemia stem cell homing and self-renewal. Cell Stem Cell. 2023;30(8):1072–e10901010.

Publisher's Note